Variation in traction forces during cell cycle progression

Benoit Vianay[1], Fabrice Senger[2], Simon Alamos[3], Maya Anjur-Dietrich[3], Elizabeth Bearce[3], Bevan Cheeseman[3], Lisa Lee[3], Manuel Théry[1,2,4]

1- Univ. Paris Diderot, INSERM, CEA, Hôpital Saint Louis, Institut Universitaire d'Hematologie, UMRS1160, CytoMorpho Lab, 75010 Paris, France.

2- Univ. Grenoble-Alpes, CEA, CNRS, INRA, Biosciences & Biotechnology Institute of Grenoble, Laboratoire de Phyiologie Cellulaire & Végétale, CytoMorpho Lab, 38054 Grenoble, France.

3- Physiology Course, Marine Biology Lab, Woods Hole

4- To whom correspondence should be addressed (email : manuel.thery@cea.fr)

Keywords :

Cell cycle, traction forces, cell mechanics.

Running title

Traction forces during cycle progression

Word count (not counting space) :

Introduction, Results and Discussion : 1585,

Materials and Methods : 586

References : 1288

Figure legends : 152

This article has been accepted for publication and undergone full peer review but has not been through the copyediting, typesetting, pagination and proofreading process, which may lead to differences between this version and the Version of Record. Please cite this article as doi: 10.1111/boc.201800006

Total : 4065

Abstract

Background Information :

Tissue morphogenesis results from the interplay between cell growth and mechanical forces. While the impact of geometrical confinement and mechanical forces on cell proliferation has been fairly well characterized, the inverse relationship is much less understood. Here we investigated how traction forces vary during cell cycle progression.

Results :

Cell shape was constrained on micropatterned substrates in order to distinguish variations in cell contractility from cell size increase. We performed traction force measurements of asynchronously dividing cells expressing a cell-cycle reporter, to obtain measurements of contractile forces generated during cell division. We found that forces tend to increase as cells progress through G1, before reaching a plateau in S phase, and then decline during G2.

Conclusions :

While cell size increases regularly during cell cycle progression, traction forces follow a biphasic behaviour based on specific and opposite regulation of cell contractility during early and late growth phases.

Significance :

These results highlight the key role of cellular signaling in the regulation of cell contractility, independently of cell size and shape. Non monotonous variations of cell contractility during cell cycle progression are likely to impact the mechanical regulation of tissue homeostasis in a complex and non-linear manner.

Introduction

Tissue morphogenesis, during both embryo development and adult tissue renewal, relies on cell growth and shape changes (Thompson, 1942; Lecuit and Lenne, 2007). Tissue growth is mostly supported by cell proliferation. The determination of tissue shape depends on the production of mechanical forces that regulate cell morphology and position (Heisenberg and Bellaïche, 2013). Tissue shape also depends on the spatial regulation of cell differentiation (Heller and Fuchs, 2015; Maitre *et al.*, 2016; Gilmour *et al.*, 2017). Cell mechanics, fate, and growth are far from independent, and the spatio-temporal coordination of growth,

differentiation and shape acquisition relies on a tight coupling between the three. It is widely-established that mechanical forces and cell shape direct cell fate and regulate cell cycle progression (Watt *et al.*, 1988; Chen *et al.*, 1997; Huang *et al.*, 1998; Ruiz and Chen, 2008; Guilak *et al.*, 2009; Klein *et al.*, 2009; Kilian *et al.*, 2010; Dupont *et al.*, 2011; Chan *et al.*, 2017).

The impact of mechanical forces on cell growth has been the focus of numerous studies, but much less is known about causality in the opposite direction ; i.e the effect of cell cycle progression on the production of mechanical forces. Cells appeared stiffer beyond S phase (Kelly *et al.*, 2011) but the magnitude of force production has not been compared between cell cycle stages. Growth factor starvation showed that quiescent cells produce less force than proliferating cells (Rape *et al.*, 2011b). The dynamics of mechanical forces produced across the cell cycle are largely unknown, though studies have nicely-characterized aspects of force production explicitly during mitosis. As cells enter mitosis, they detach from the extra-cellular matrix in a process called deadhesion (Marchesi *et al.*, 2014) resulting in a drastic reduction of tractional forces (Lesman *et al.*, 2014). Mitotic cells continue to produce contractile forces, but they are distributed internally and lead to cell rounding and stiffening (Maddox and Burridge, 2003; Théry and Bornens, 2008; Stewart *et al.*, 2011). Cells regain the ability to produce traction forces as they exit from mitosis and respread onto the extra-cellular matrix in early G1 (Cramer and Mitchison, 1995; Lesman *et al.*, 2014).

It is not known how traction forces vary from early G1 to late G2. The null hypothesis is that they remain constant, however, the main characteristic of cell cycle progression is cell growth: cell size and mass increase steadily from early G1 to late G2 (Kafri *et al.*, 2013; Son *et al.*, 2015; Varsano *et al.*, 2017). Several works have shown that cell size has a clear influence on the production of traction forces, and that bigger cells tend to produce larger forces (Tan *et al.*, 2003; Reinhart-king *et al.*, 2005; Tolić-Nørrelykke and Wang, 2005; Rape *et al.*, 2011a; Oakes *et al.*, 2014). According to this trend, traction forces should increase steadily with cell cycle progression. We took advantage of a two-week rotation during the Physiology course in Woods Hole to test these hypotheses, and measure the evolution of traction forces during cell cycle progression.

Results and Discussion

One straightforward strategy to assess traction forces across the cell cycle would rely on synchronizing cells and performing force production measurements during each cell cycle stage. However synchronizing drugs, which inhibit specific cyclin kinases, blocks DNA replication or disassemble microtubules (Ma and Poon, 2017), can interfere with normal cell cycle progression after release (Bar-Joseph *et al.*, 2008). Rather than pharmacologically perturbing the cell cycle to induce synchronization, we opted to utilize asynchronous cells expressing the fluorescent ubiquitin-based cell cycle indicator (FUCCI) reporter system. The FUCCI reporter is based on the sequential hCdt1-mCherry expression in G1 and hGem-Azami Green expression in S/G2/M (Sakaue-Sawano *et al.*, 2008). We worked with RPE-1 cells, a diploid, nontransformed

human epithelial cell line, stably expressing the Fucci constructs (Ganem *et al.*, 2014) (Figure S1A). Cells were plated on soft poly-acrylamide gel with embedded fiducial beads, to visualize gel deformation and infer the traction forces produced by the cells, as previously described (Dembo and Wang, 1999) (Figure S1B). It is important to plate cells at low density in order to detect their individual traction force field. However, RPE1 cells are motile in these conditions, and migration is a great source of variability in force production (Meili *et al.*, 2010; Chang *et al.*, 2013; Leal-Egaña *et al.*, 2017). In order to limit these large variations that could blur the changes due to cell cycle progression, cells were plated on adhesive micropatterns, which prevented their motion and normalized their morphology, to achieve a constant and reproducible shape (Singhvi *et al.*, 1994; Théry, 2010). We further considered that standardizing stress fiber position and number would reduce inter-cellular variability (Mandal *et al.*, 2014). We achieved this by plating cells on 60-micron-long and 12-micro-wide dumbell-shaped micropatterns, in which the shape and position of non-adhesive regions dictate the number, size and position of stress fibers (Théry *et al.*, 2006) (Figure S1C). The combination of these methods: the Fucci reporter, the deformable substrate and the controlled cell shape, allowed us to measure cell cycle position and traction forces in standardized conditions (Figure 1A).

We first confirmed that cells displayed the expected color changes as they progressed in the cell cycle when micropatterned on poly-acrylamide gel (Figure S2). Fibronectin-coated micropatterns were first manufactured on glass coverslips, and then transferred onto a poly-acrylamide hydrogel (Vignaud *et al.*, 2014) (see Methods). RPE1-Fucci cells were plated on micropatterned gels and monitored 24h using time-lapse confocal microscopy. As expected, cells expressing exclusively the hCdt1-mCherry (red) construct at the beginning of the cell cycle, reduced it progressively over time, and increased the production of hGem-Azami Green, resulting in the exclusive production of hGem-Azami Green approximately 12hrs later, at the end of S phase (Figure S2A). This « green » phase, which corresponded to the G2 phase, lasted about five hours until entry into mitosis (Figure S2A). These durations approximately correspond to the cell cycle durations reported for this cell line (Azimzadeh *et al.*, 2009). When the fluorescence signal of each reporter is plotted over time for individual cells, their trajectories follow the typical, dome-like, trend of normal cell cycle progression (Figure S2B, to be compared to Figure 1G in (Sakaue-Sawano *et al.*, 2008)). The relationship between fluorescence ratio and cell cycle stage (Sakaue-Sawano *et al.*, 2008) was used to define the boundaries separating the various cell cycle stages : early G1, late G1, S and G2 phase (Figure S2B).

Once the cell cycle stage had been determined by measuring the fluorescence intensities of the two reporters, we imaged the dark-red-fluorescent beads that were embedded in the poly-acrylamide gel, to obtain their position while under tension. Cells were then treated with trypsin to disengage the traction forces that were applied on the substrate, and allow relaxation of the fiducial beads. Images of the beads in the presence and absence of cell-mediated tension were processed in order to measure their auto-correlation function and deduce the gel deformation field (Tseng *et al.*, 2012; Martiel *et al.*, 2015) (see Methods). We then used Fourier-transform traction cytometry to estimate the corresponding cell traction force field (Butler *et al.*,

2002; Martiel *et al.*, 2015). (Figure 1B). The force field was further used to calculate the total traction energy produced by each individual cell, to generate the substrate deformation we observed (Butler *et al.*, 2002; Martiel *et al.*, 2015). We then combined the measure of cell cycle position (Figure 1C) and the values of traction energies for each individual cell, to plot the variations of traction forces with respect to cell cycle progression (Figure 1D). We observed a biphasic evolution of traction forces. Traction forces first increased from early G1 to late G1 and S phase (Figure 1D). More surprisingly, traction forces then dropped after S phase until G2 (Figure 1D).

The increase of forces from G1 to S is consistent with previous predictions relating cell area and contractility (Tan *et al.*, 2003; Reinhart-king *et al.*, 2005; Tolić-Nørrelykke and Wang, 2005; Rape *et al.*, 2011a; Oakes *et al.*, 2014), based on the fact that cell mass and volume increase from G1 to S phase (Son *et al.*, 2015; Varsano *et al.*, 2017). However, in our experimental setting, cell area is predetermined by the micropatterned substrate ; effectively uncoupling cell cycle progression from the contact area. Since all cells had the exact same spreading and adhesion areas, the increase in traction forces must reflect a genuine activation of the traction force machinery from early G1 to S phase. The force reduction after S phase was unexpected, given that cell mass and volume keep increasing during this period (Kafri *et al.*, 2013; Son *et al.*, 2015; Varsano *et al.*, 2017). These force variations may reflect changes in integrin activation. Indeed, integrins are specifically activated by growth factors during G1 (Walker and Assoian, 2005) and they are known to activate downstream signaling pathways leading to acto-myosin contractility (Harburger and Calderwood, 2009). So the G1 phase may be more effective in force production than the others. After the G1/S transition, cells are committed to mitosis and their progression is irreversible. In S and G2, cells are no longer sensitive to growth factors. The off-switching of their receptors is likely to impact the integrin activation and be responsible for the reduction in forces that we observed. The signaling pathways and the molecular players connecting cell cycle progression to the regulation of focal adhesions and force production mechanism (Livne and Geiger, 2016) remain to be investigated.

Finally, it seems important to extend our study on single cells to the tissue level in future works. How do intercellular tensional forces vary during cell cycle progression? How do cells sense the changes in traction and tension in their neighbours? Does it impact their own cell cycle progression? Do cells distinguish the mechanical state of their neighbours in early G1 or G2 ? What are the respective contribution of cell size and cell contraction ? Addressing these questions would shine some light on the physical and biochemical mechanisms involved in the mechanical regulation of tissue homeostasis.

Materials and Methods

Cell lines

RPE1-FUCCI (provided by the lab of David Pellman) were grown in a humidified incubator at 37°C and 5% CO_2 in DMEM/F12 medium supplemented with 10% fetal bovine serum and 1% penicillin/streptomycin. All cell culture products were purchased from GIBCO/Life technologies.

Cells were seeded on patterned gels at 100,000 cells/cm^2. Non-adherent cells were washed away as soon as cells started to attach to the micropatterns. Cells were then allowed to spread fully onto the patterns for 3 hours.

Hydrogel Micropatterning

Detailed procedure has been described elsewhere for glass micropatterning (Azioune *et al.*, 2010), and gel micropatterning (Vignaud *et al.*, 2014). In brief, micropatterns were first made on glass coverslip and then transferred onto poly-acrylamide gels.

Glass coverslips were oxidized by oxygen plasma (PDC-100-HP Harrick Plasma) (10 sec, 30 W) and incubated for 30 min. with 0.1 mg/ml PLL-g-PEG (PLL20K-G35-PEG2K, JenKem) in 10mM HEPES pH 7.4. Dried coverslips where then exposed to deep-UV (PSD Pro series NOVASCAN) through a photomask (Toppan) for 4 min. After UV treatment, coverslips were incubated with 10 µg/ml fibronectin (Sigma) and 10 µg/ml Alexa Fluor 546 fibrinogen conjugate (Invitrogen) in 100mM Sodium Bicarbonate buffer, pH=8.4, for 30 min then washed in 100mM Sodium Bicarbonate buffer, pH=8.4 and finally dried.

Fluorescent beads were passivated by mixing 50µl of beads (Fluorosphere #8810, Invitrogen) in 1 ml of PLL-PEG (0.1 $mg.ml^{-1}$, JenKem Technology) for 1 H at 4°C. Beads were washed 3 times in 10 mM HEPES pH 7.4 and resuspended in 150 µl washing buffer. Acrylamide (8%) and bis-acrylamide solution (0.48%) (Sigma) was degassed for 30 min, and mixed with 10µL of passivated beads by sonication before addition of APS and TEMED. A drop of 25 µl of this mix was sandwiched between the micropatterned coverslip and a silanised (acryl-silane) glass coverslip and let to polymerize for 30 min. Gel was allowed to swell in 100mM sodium bicarbonate buffer and gently removed. Coverslip were rinced with PBS before cell plating.

The Young-modulus of the gels was estimated around 40kPa given the relative amounts of acrylamide and bis-acrylamide (Tse and Engler, 2010).

Imaging

Live microscopy was performed on Zeiss Cell Observer Z inverted microscopes with Hamamatsu Orca flash 4.0 cameras. Fucci nuclei in time and force measurement experiments were aquired respectively with a 40x (NA=1.2) and a 63x Plan Apo (NA=1.4) objectives.

Nuclei normalized colors, Rn and Gn, were obtained by measuring each fluorescence intensity in a 5µm diameter circle manually located in the brightest part of the cell nucleus ; then divided by its respective background, measured from a 5µm diameter circle manually located far from the cell.

Traction Force Microscopy

We used the ImageJ plugin and followed the procedure previously described (Martiel *et al.*, 2015). Displacement fields were obtained from bead images taken before and after removal of cells by trypsin treatment. Images were first aligned to correct for experimental drift then cropped to produce 1000 px X 1000 px images. Displacement field was calculated by particle imaging velocimetry (PIV) on the base of normalized cross-correlation following an iterative scheme. Final grid size was 1.65 µm X 1.65 µm. Erroneous vectors where discarded owing to their low correlation value and replaced by the median value of the neighbouring vectors. Traction-force field was subsequently estimated by Fourier Transform Traction Cytometry, with a regularization parameter set to $9x10^{-10}$. The mechanical energy was calculated by summing the dot products of displacement with the force times the grid area: 2.72 μm^2.

Acknowledgements

We thank the Physiology course directors Jennifer Lippincott-Schwartz, Wallace Marshall and Rob Phillips for inviting all of us to the Marine Biology Laboratory in Woods Hole. We also thank them for their great support, thoughtful advice and remarkably good and motivating intuitions. We are very grateful to Carolyn Ott, Adam Catching and Steve Wilbert who were more than helpful both day and night, during these two weeks. We thank Neil Ganem and David Pellman for providing us the RPE1-Fucci cell line. We thank Aldo Ferrari and the Laboratory of Thermodynamics in Emerging Technologies for sharing with us unpublished data that were consistent with the results we reported here.

The authors have no conflict of interest to declare.

Authors contribution

All authors performed the experiments together; BV double-checked all force measurements; MT designed the project and wrote the manuscript.

References

Azimzadeh, J., Hergert, P., Delouvée, A., Euteneuer, U., Formstecher, E., Khodjakov, A., and Bornens, M. (2009). hPOC5 is a centrin-binding protein required for assembly of full-length centrioles. J. Cell Biol. *185*, 101–114.

Azioune, A., Carpi, N., Tseng, Q., Théry, M., and Piel, M. (2010). Protein micropatterns: A direct printing protocol using deep UVs. Methods Cell Biol. *97*, 133–146.

Bar-Joseph, Z., Siegfried, Z., Brandeis, M., Brors, B., Lu, Y., Eils, R., Dynlacht, B. D., and Simon, I. (2008). Genome-wide transcriptional analysis of the human cell cycle identifies genes differentially regulated in normal and cancer cells. Proc.Natl.Acad.Sci.U.S.A *105*, 955–960.

Butler, J. P., Tolić-Nørrelykke, I. M., Fabry, B., and Fredberg, J. J. (2002). Traction fields, moments, and strain energy that cells exert on their surroundings. Am. J. Physiol. Cell Physiol. *282*, C595-605.

Chan, C. J., Heisenberg, C., and Hiiragi, T. (2017). Coordination of Morphogenesis and Cell-Fate Specification in Development. Curr. Biol. *27*, 1–12.

Chang, S. S., Guo, W., Kim, Y., and Wang, Y. (2013). Guidance of Cell Migration by Substrate Dimension. Biophysj *104*, 313–321.

Chen, C. S., Mrksich, M., Huang, S., Whitesides, G. M., and Ingber, D. E. (1997). Geometric Control of Cell Life and Death. Science (80-.). *276*, 1425–1428.

Cramer, L. P., and Mitchison, T. J. (1995). Myosin is involved in postmitotic cell spreading. J. Cell Biol. *131*, 179–189.

Dembo, M., and Wang, Y. (1999). Stresses at the Cell-to-Substrate Interface during Locomotion of Fibroblasts. Biophys. J. *76*, 2307–2316.

Dupont, S. *et al.* (2011). Role of YAP / TAZ in mechanotransduction.

Ganem, N. J., Cornils, H., Chiu, S.-Y., O'Rourke, K. P., Arnaud, J., Yimlamai, D., Théry, M., Camargo, F. D., and Pellman, D. (2014). Cytokinesis Failure Triggers Hippo Tumor Suppressor Pathway Activation. Cell *158*, 833–848.

Gilmour, D., Rembold, M., and Leptin, M. (2017). From morphogen to morphogenesis and back. Nature *541*, 311–320.

Guilak, F., Cohen, D. M., Estes, B. T., Gimble, J. M., Liedtke, W., and Chen, C. S. (2009). Control of stem cell fate by physical interactions with the extracellular matrix. Cell Stem Cell *5*, 17–26.

Harburger, D. S., and Calderwood, D. a. (2009). Integrin signalling at a glance. J. Cell Sci. *122*, 1472–1472.

Heisenberg, C.-P., and Bellaïche, Y. (2013). Forces in Tissue Morphogenesis and Patterning. Cell *153*, 948–962.

Heller, E., and Fuchs, E. (2015). Tissue patterning and cellular mechanics. J. Cell Biol. *211*, 219–231.

Huang, S., Chen, C. S., and Ingber, D. E. (1998). Control of Cyclin D1 , p27 Kip1 , and Cell Cycle Progression in Human Capillary Endothelial Cells by Cell Shape and Cytoskeletal Tension. Mol. Biol. Cell *9*, 3179–3193.

Kafri, R., Levy, J., Ginzberg, M. B., Oh, S., Lahav, G., and Kirschner, M. W. (2013). Dynamics extracted from fixed cells reveal feedback linking cell growth to cell cycle. Nature *494*, 480–483.

Kelly, G. M., Kilpatrick, J. I., van Es, M. H., Weafer, P. P., Prendergast, P. J., and Jarvis, S. P. (2011). Bone cell elasticity and morphology changes during the cell cycle. J. Biomech. *44*, 1484–1490.

Kilian, K. a, Bugarija, B., Lahn, B. T., and Mrksich, M. (2010). Geometric cues for directing the differentiation of mesenchymal stem cells. Proc. Natl. Acad. Sci. U. S. A. *107*, 4872–4877.

Klein, E. a, Yin, L., Kothapalli, D., Castagnino, P., Byfield, F. J., Xu, T., Levental, I., Hawthorne, E., Janmey, P. a, and Assoian, R. K. (2009). Cell-cycle control by physiological matrix elasticity and in vivo tissue stiffening. Curr. Biol. *19*, 1511–1518.

Leal-Egaña, A., Letort, G., Martiel, J.-L., Christ, A., Vignaud, T., Roelants, C., Filhol, O., and Théry, M. (2017). The size-speed-force relationship governs migratory cell response to tumorigenic factors. Mol. Biol. Cell, mbc.E16-10-0694.

Lecuit, T., and Lenne, P.-F. (2007). Cell surface mechanics and the control of cell shape, tissue patterns and morphogenesis. Nat. Rev. Mol. Cell Biol. *8*, 633–644.

Lesman, A., Notbohm, J., Tirrell, D. A., and Ravichandran, G. (2014). Contractile forces regulate cell division in three-dimensional environments. J. Cell Biol. *205*, 155–162.

Livne, A., and Geiger, B. (2016). The inner workings of stress fibers - from contractile machinery to focal adhesions and back. J. Cell Sci. *129*, 1293–1304.

Ma, H. T., and Poon, R. Y. C. (2017). Synchronization of HeLa Cells. 189–201.

Maddox, A. S., and Burridge, K. (2003). RhoA is required for cortical retraction and rigidity during mitotic cell rounding. J. Cell Biol. *160*, 255–265.

Maitre, J.-L., Turlier, H., Illukkumbura, R., Eismann, B., Niwayama, R., Nédélec, F., and Hiiragi, T. (2016). Asymmetric division of contractile domains couples cell positioning and fate specification. Nature *536*, 344–348.

Mandal, K., Wang, I., Vitiello, E., Orellana, L. A. C., and Balland, M. (2014). Cell dipole behaviour revealed by ECM sub-cellular geometry. Nat. Commun.

Marchesi, S., Montani, F., Deflorian, G., D'Antuono, R., Cuomo, A., Bologna, S., Mazzoccoli, C., Bonaldi, T.,

DiFiore, P. P., and Nicassio, F. (2014). DEPDC1B coordinates de-adhesion events and cell-cycle progression at mitosis. Dev. Cell *31*, 420–433.

Martiel, J.-L., Leal, A., Kurzawa, L., Balland, M., Wang, I., Vignaud, T., Tseng, Q., and Théry, M. (2015). Measurement of cell traction forces with ImageJ. Methods Cell Biol. *125*, 269–287.

Meili, R., Alonso-Latorre, B., del Alamo, J. C., Firtel, R. A., and Lasheras, J. C. (2010). Myosin II Is Essential for the Spatiotemporal Organization of Traction Forces during Cell Motility. Mol. Biol. Cell *21*, 405–417.

Oakes, P. W., Banerjee, S., Marchetti, M. C., and Gardel, M. L. (2014). Geometry Regulates Traction Stresses in Adherent Cells. Biophys. J. *107*, 825–833.

Rape, A. D., Guo, W.-H., and Wang, Y.-L. (2011a). The regulation of traction force in relation to cell shape and focal adhesions. Biomaterials *32*, 2043–2051.

Rape, A., Guo, W.-H., and Wang, Y.-L. (2011b). Microtubule depolymerization induces traction force increase through two distinct pathways. J. Cell Sci. *124*, 4233–4240.

Reinhart-king, C. A., Dembo, M., and Hammer, D. A. (2005). The Dynamics and Mechanics of Endothelial Cell Spreading. Biophys. J. *89*, 676–689.

Ruiz, S. A., and Chen, C. S. (2008). Emergence of patterned stem cell differentiation within multicellular structures. Stem Cells *26*, 2921–2927.

Sakaue-Sawano, A. *et al.* (2008). Visualizing Spatiotemporal Dynamics of Multicellular Cell-Cycle Progression. Cell *132*, 487–498.

Singhvi, R., Kumar, a, Lopez, G. P., Stephanopoulos, G. N., Wang, D. I., Whitesides, G. M., and Ingber, D. E. (1994). Engineering cell shape and function. Science *264*, 696–698.

Son, S., Kang, J. H., Oh, S., Kirschner, M. W., Mitchison, T. J., and Manalis, S. (2015). Resonant microchannel volume and mass measurements show that suspended cells swell during mitosis. J. Cell Biol. *211*, 757–763.

Stewart, M. P., Helenius, J., Toyoda, Y., Ramanathan, S. P., Muller, D. J., and Hyman, A. A. (2011). Hydrostatic pressure and the actomyosin cortex drive mitotic cell rounding. Nature *469*, 226–230.

Tan, J. L., Tien, J., Pirone, D. M., Gray, D. S., Bhadriraju, K., and Chen, C. S. (2003). Cells lying on a bed of microneedles: an approach to isolate mechanical force. Proc. Natl. Acad. Sci. U. S. A. *100*, 1484–1489.

Théry, M. (2010). Micropatterning as a tool to decipher cell morphogenesis and functions. J. Cell Sci. *123*, 4201–4213.

Théry, M., and Bornens, M. (2008). Get round and stiff for mitosis. HFSP J. *2*, 65–71.

Théry, M., Pépin, A., Dressaire, E., Chen, Y., and Bornens, M. (2006). Cell distribution of stress fibres in response to the geometry of the adhesive environment. Cell Motil. Cytoskeleton *63*, 341–355.

Thompson, D. W. (1942). On Growth and Form, Cambridge Univ. Press.

Tolić-Nørrelykke, I. M., and Wang, N. (2005). Traction in smooth muscle cells varies with cell spreading. J. Biomech. *38*, 1405–1412.

Tse, J. R., and Engler, A. J. (2010). Preparation of hydrogel substrates with tunable mechanical properties. Curr. Protoc. Cell Biol. *Chapter 10*, Unit 10.16.

Tseng, Q., Duchemin-Pelletier, E., Deshiere, A., Balland, M., Guillou, H., Filhol, O., and Théry, M. (2012). Spatial organization of the extracellular matrix regulates cell-cell junction positioning. Proc. Natl. Acad. Sci. U. S. A. *109*, 1506–1511.

Varsano, G., Wang, Y., and Wu, M. (2017). Probing Mammalian Cell Size Homeostasis by Channel-Assisted Cell Reshaping. Cell Rep. *20*, 397–410.

Vignaud, T., Ennomani, H., and Théry, M. (2014). Polyacrylamide hydrogel micropatterning. Methods Cell Biol. *120*, 93–116.

Walker, J. L., and Assoian, R. K. (2005). Integrin-dependent signal transduction regulating cyclin D1 expression and G1 phase cell cycle progression. Cancer Metastasis Rev *24*, 383–393.

Watt, F. M., Jordan, P. W., and O'Neill, C. H. (1988). Cell shape controls terminal differentiation of human epidermal keratinocytes. Proc. Natl. Acad. Sci. U. S. A. *85*, 5576–5580.

Figure 1: Traction forces variation during cell cycle progression

A) Experimental set up based on FUCCI cells spread on micro patterned PAA gels to measure cell traction forces during cell cycle progression.

B) Micropatterned RPE1 cells expressing Fucci construct. Phase contrast images were overlaid with red and green fluorescence images (top row). Examples show distinct cells in early G1, late G1, S and G2 with their corresponding traction force fields (bottom row). Arrows represent the local force magnitude and orientation. Force scale bar is in Pascal.

C) Log-log diagram of the nuclear Fucci fluorescence. The graph shows normalized red color in function of the normalized green color. Each point represents a cell (n=66, N=3 independant experiments). The dashed lines separate cycle phases (see Figure S2)

D) Comparison of the mechanical traction energies produced by cells in early G1, late G1, S and G2. Groups were defined in panel B. Bars represent mean values and error bars the standard deviations (** p<0.01).

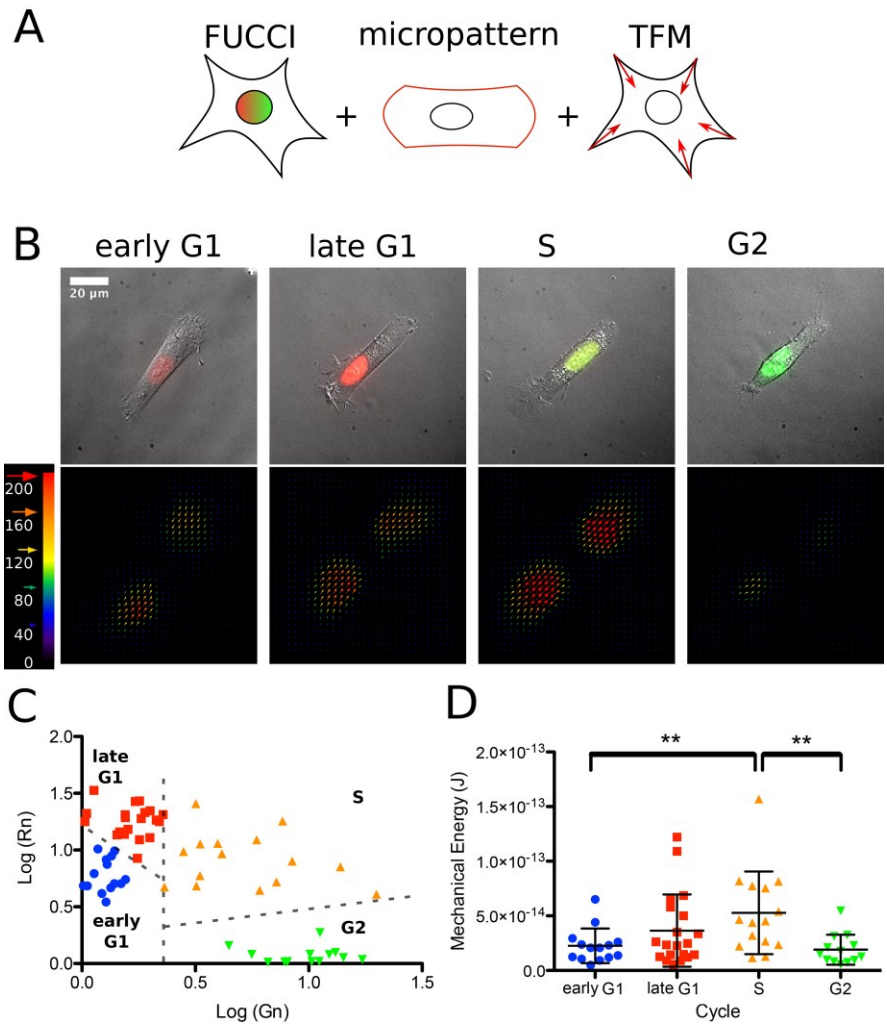

Graphical abstract

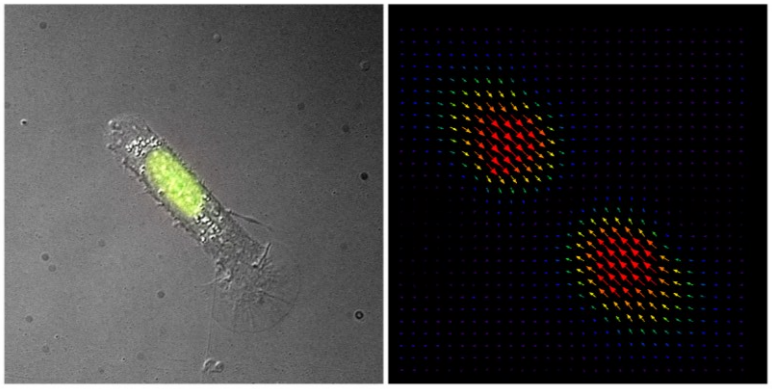

This manuscript compares cell traction forces according to their position in their cell cycle. It shows that forces increase from early G1 to S phase. It then reveals an unexpected decrease of traction forces from S to G2.